Comparative study of tetracycline degradation efficiency using peroxydisulfate activated with sludge biochar and activated coke: the role of surface defects

Guoting Li[a,*], Huan Chen[a], Taiyang Cao[a], Xiangping Ran[a], Yujie Guo[a], Chenliang Shen[b], Yingxu Liu[c], Tannaz Pak[d]

[a]*School of Environmental and Municipal Engineering, North China University of Water Resources and Electric Power, Zhengzhou 450046, China, Tel.: +86-371-69127538; Fax: +86-371-65790239; emails: lipsonny@163.com (G. Li), 15690865875@163.com (H. Chen), xiaocao910@foxmail.com (T. Cao), ranxp0610@126.com (X. Ran), guoyujie@ncwu.edu.cn (Y. Guo)*
[b]*Zhongzhou Water Holding Co., Ltd., Zhengzhou 450046, China, email: shenchenl@126.com (C. Shen)*
[c]*Zhengzhou Sewage Purifying Co., Ltd., Zhengzhou 450000, email: 358918109@qq.com (Y. Liu)*
[d]*School of Computing, Engineering, and Digital Technologies, Teesside University, Borough Road, Middlesbrough, TS1 3BX, UK, email: t.pak@tees.ac.uk (T. Pak)*

ABSTRACT

Both sludge biochar (BC) and activated coke (ACO) are hierarchical while their surface properties have a large disparity. We show that sludge biochar pyrolyzed at 600°C (BC600) outperforms biochar produced at other temperatures for a range of biomass feedstock. BC600 displays lower carbon content, lower surface area, and importantly more abundant surface oxygen-containing functional groups when compared with ACO. BC600 and ACO were used to activate peroxydisulfate (PDS) for tetracycline oxidation while the degradation mechanisms were comprehensively discussed. Interestingly, ACO demonstrated a particularly higher performance where activating PDS compared with BC600. The K_{app} value for the synergetically combined ACO-PDS process was 2.15 times that of the sum of adsorption and PDS oxidation processes alone, while it was 1.72 times for the BC600-PDS process. Solution pH had a more dramatic influence on BC600 than on ACO. Quenching experiments proved that both $OH^\bullet$ and $SO_4^{\bullet-}$ contributed insignificantly while most of the degradation was attributed to superoxide radical ($O_2^{\bullet-}$), singlet oxygen ($^1O_2$), and active holes (h^+). After reducing carbonyl groups on both carbons by KBH_4 in absolute alcohol, quenching experiments did not indicate the key role of carbonyl groups for $^1O_2$ generation. Non-radical pathway proved dominant in the carbon/PDS catalytic process. Excellent reusability and stability for ACO was observed in repeated use experiments.

Keywords: Peroxydisulfate; Activation mechanism; Activated coke; Sludge biochar; Tetracycline

1. Introduction

Concerning removal of organic contaminants from water and wastewater, advanced oxidation processes demonstrate their unique advantages over other techniques including bio-treatment and adsorption process. As to the organic contaminants especially in extremely low concentration, which is mainly the so-called micro-pollutants, most of the techniques cannot remove them efficiently and cost-effectively. For example, the conventional techniques for tetracycline removal such as bio-treatment, sedimentation, sand filtration, flocculation, and coagulation are not so efficient as expected, while tetracycline is always detected in the effluent from wastewater treatment plant

* Corresponding author.

[1]. Adsorption process proves to be incapable of removing micro-pollutants cost-effectively as it will consume a large amount of adsorbents as a result of the established low-concentration equilibrium. By contrast, advanced oxidation process (AOPs) such as persulfate oxidation are utilized for effective removal of antibiotics including tetracycline [2,3]. The organic contaminants can be completely decomposed or mineralized into CO_2 and H_2O by a series of strong oxidizing species generated in these AOPs [4,5]. Even though the oxidants involved might be quite expensive, the application of AOPs for low-concentration contaminants removal is still cost-effective to some extent.

Recent study has demonstrated that persulfate activation system is one of the most promising AOPs subjected to practical application. On one hand, the application of persulfate is more economical than other commercial oxidants ($0.74/kg vs. $1.5/kg of hydrogen peroxide). The storage and transportation of persulfate is quite more convenient compared to other oxidants such as hydrogen peroxide and ozone [6]. On the other hand, a series of strong oxidizing species including $SO_4^{\bullet-}$, $OH^{\bullet}$, $O_2^{\bullet-}$, and $^1O_2$ are always generated concurrently in peroxydisulfate (PDS) activation process. The oxidation potential of $SO_4^{\bullet-}$, $OH^{\bullet}$, $O_2^{\bullet-}$ and $^1O_2$ are 2.5~3.1, 2.7, 2.6 and 1.88 V, respectively [7]. $SO_4^{\bullet-}$ has significant advantages over $OH^{\bullet}$ for the degradation of contaminants with higher oxidation potential, longer life span (30~40 µs vs. 1 µs) and higher degradation efficiency [8]. These oxidizing species are quite capable of decomposing organic contaminants into CO_2 and H_2O. Persulfate, as the source of $SO_4^{\bullet-}$, can be effectively activated through various ways such as thermal activation [9], ultraviolet (UV) activation [10], alkali activation [11], ultrasonic activation [12], transition metal activation [13,14] and electro-activation [15,16]. Totally, the persulfate activation system is characterized with high efficiency, low cost and environment-friendliness in nature.

Metal ions and metal oxides were used to efficiently catalyze persulfate while the use of metal-based catalyst might result in metal leaching. A number of researches have demonstrated that carbonaceous materials including carbon nanotube, activated carbon, graphene and biochar have been reported to be capable of activating persulfate for high-efficiency degradation of organics. As to these carbonaceous materials, surface area, zig-zag edges/defect structure and surface oxygen-containing functional groups are considered to be the primary influencing factors for catalytic performance [17–19]. It is well known that PDS activation by metal-based catalyst undergoes a free radical-based oxidation mechanism, while there is still a bitter controversy concerning metal-free catalyst [20]. Although some researchers reported that the carbon-driven persulfate activation system was always dominated by non-radical pathways [21], it always falls into discrepancy when discussing the underlying activation and oxidation mechanism. Some researchers reported that the possible active sites include oxygen functional groups, heteroatom configurations, and sp^2-hybridized carbon matrix. The underlying mechanisms involving surface bound radicals, singlet oxygen ($^1O_2$), and metastable persulfate-catalyst complexes were proposed based on the results of scavenging experiments and electron spin resonance spectrometry detection [22,23].

Among these carbonaceous materials, activated carbon and biochar are the most studied metal-free catalyst applied in persulfate activation system. Activated coke (ACO) is a carbonaceous material used as a substitute for activated carbon. ACO is usually featured by its macro- and mesoporous carbon structures [24,25]. It has been well applied in advanced treatment of secondary effluent in Zhengzhou, China. Meanwhile, as a kind of low-cost carbon derived from abundant and renewable waste biomasses, biochar has attracted increasing concern for application in water treatment and soil remediation based on its typical mesoporous structure [26]. As one of the typical municipal wastes, a huge amount of activated sludge is generated from biological wastewater treatment annually, and utilization of sludge biochar might be an ideal choice for practical water and wastewater treatment. As biochar has excellent surface properties including abundant surface functional groups and comparatively high surface area, biochar can catalyze the conversion of different oxidants to reactive oxygen species for *in-situ* chemical oxidation (ISCO) of various organic contaminants [27]. Basically, the structure and surface properties of carbonaceous materials play a vital role for activating persulfate. It is reported that the characteristics of a carbon catalyst even determine the radical pathway, non-radical pathway, adsorption and cleavage of pollutants [28]. In this research, both sludge biochar and ACO were comparatively used for ISCO degradation of tetracycline by activating PDS. After reducing of carbonyl groups on both carbons by KBH_4, the roles of carbonyl are investigated by quenching methods. The roles of surface oxygen-containing functional groups and defects are profoundly discussed herein.

2. Materials and methods

2.1. Materials

Potassium peroxydisulfate (PDS, $K_2S_2O_8$, purity ≥ 99.5%) was provided by ANPEL Laboratory Technologies Reagent Inc., (Shanghai, China). Tetracycline (TC) was purchased from Hefei Bomei Biological Science and Technology Co., Ltd., (Anhui Province, China) and used without further purification. Activated coke (ACO) was provided by Zhengzhou Sewage Purification Co., Ltd., (Zhengzhou, China). Ethylenediaminetetraacetic acid disodium salt (EDTA-2Na) used as a hole scavenger was bought from Guangfu Technology Development Co., Ltd., (Chengdu, China). Other chemicals including 1,4-benzoquinone (Bq) and KBH_4 were purchased from Maclin Co., Ltd., (Shanghai, China). Deionized (DI) water was used to prepare solutions throughout the study.

2.2. Preparation of biochars derived from activated sludge

Municipal activated sludge was collected from the dewatering stage of Matougang wastewater treatment plant (Zhengzhou City, China). The detailed preparation procedures of sludge biochar can be referred to our previous study [29]. Considering a high ash content within the resultant sludge biochar (BC), all the biochar samples were demineralized in a 4 mol·L⁻¹ HCl solution and separated by filtration. After that, the demineralized biochars were rinsed with DI

water until a neutral solution pH and oven-dried overnight at 80°C for further use. These sludge biochars pyrolyzed at 200°C, 300°C, 400°C, 500°C, and 600°C were hereafter designated as BC200, BC300, BC400, BC500 and BC600, respectively wherein the suffix number represented the pyrolytic temperature.

2.3. Preparation of KBH₄-reduced carbon

In 20 mL absolute alcohol, 2.0 g of sludge biochar BC600 or ACO were treated by 0.1 g KBH₄ for 2 h to reduce the carbonyl groups (–C=O) into C–OH groups so as to check the role of carbonyl groups during PDS catalytic process.

2.4. Characterization

The surface morphologies of the sludge biochar BC600 and ACO were characterized by a Philips Quanta-2000 scanning electron microscope coupled with an energy-dispersive X-ray (EDX) spectrometer (Philips Quanta 2000, Netherlands). Surface functional groups of these biochars were recorded on a Nicolet NEXUS 470 FTIR spectrophotometer from 400 to 4,000 cm⁻¹ (Nicolet NEXUS 470 FTIR spectrophotometer, USA). The specific surface areas of BC600 and ACO were measured by nitrogen adsorption/desorption using Brunauer–Emmett–Teller (BET) method with a surface area and pore size analyzer (NOVA 2200e, USA). The acidic functional groups, including carboxyl, lactonic, and phenolic groups on the sludge biochar BC600 and ACO were determined using Boehm's titration method [30,31]. The zeta potentials of BC600 and ACO were determined by using a zeta potential analyzer (Zetasizer NANO ZS90, Malvern Co., UK).

2.5. Batch degradation experiment

The PDS catalytic performance of BC600 and ACO were evaluated by mixing 10 mg of carbonaceous catalyst with 100 mL TC solution (10 mg·L⁻¹) and a certain amount of PDS simultaneously. The mixture was magnetically stirred at a constant speed and room temperature for 60 min. Samples were collected at desired time intervals and quenched with sodium thiosulfate before determination. All solution pH values were maintained at neutral pH except for the study of pH effect. Solution pH adjustment was conducted by addition of a dilute HCl or NaOH solution.

2.6. Analysis methods

Samples were collected and filtered through a 0.45 μm membrane before analysis. The TC concentration of the samples was determined by measuring the absorbance at its maximum absorbance wavelength of 360 nm by an UVmini-1240 spectrophotometer (Shimadu, Japan).

The pseudo-first-order kinetics for TC degradation was simulated as:

$$\ln\left(\frac{C_0}{C_t}\right) = K_{app}t \tag{1}$$

where C_t is the TC concentration at time t, C_0 is the initial TC concentration, and K_{app} is the apparent first-order rate constant (min⁻¹).

The decrease of apparent rate constant (pseudo-first-order) K_{app} resulted from scavengers quenching can be used to indicate the contribution and contribution percentages of oxidizing species including hydroxyl radicals, which were calculated as the following equations [32]:

$$\text{Contribution } K_{app} = K_{app} - K_{app}\left(\text{quenching}\right) \tag{2}$$

$$\text{Contribution percentage} = \left(\frac{1 - K_{app}\left(\text{quenching}\right)}{K_{app}}\right) \times 100\% \tag{3}$$

3. Results and discussion

3.1. Selection of biochar for PDS catalysis

3.1.1. Catalytic performance of biochars derived from different biomasses

Various biochars derived from activated sludge, sugarcane bagasse, platanus orientalis bark, lignocellulose, and rice straw were employed for the removal of TC by adsorption and PDS catalytic process. Considering surface properties and stability of biochars, the biochars pyrolyzed at 600°C (BC600) was compared herein. As illustrated in Fig. 1, not all the biochars could enhance the PDS oxidation process efficiently as only biochars derived from lignocellulose, activated sludge and rice straw had a higher K_{app} value of PDS catalytic process than that of adsorption. The adsorption and PDS catalytic capability of sludge biochar BC600 outperformed other biochars apparently. Meanwhile, the K_{app} values for the PDS oxidation alone, sludge biochar BC600 adsorption alone and the combined process were of 1.19×10^{-3}, 6.01×10^{-3} and 1.24×10^{-2} min⁻¹ ($R^2 = 0.890$, 0.885 and 0.972), respectively. The K_{app} value of the combined process is 1.72 times that of PDS oxidation and adsorption alone, indicating an evident synergetic effect. The above implies that sludge biochar BC600 could be a good carbon candidate for activating PDS.
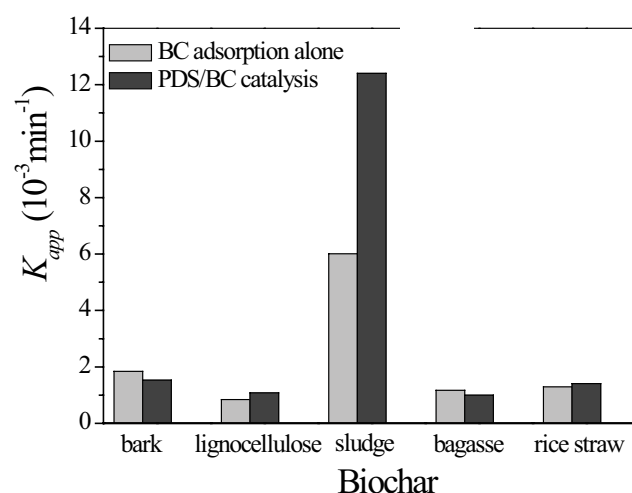

Fig. 1. Adsorption and PDS activation capability of various biochars: PDS 30 mg·L⁻¹, BC600 dose 10 mg.

3.1.2. Effect of pyrolytic temperature for sludge biochar synthesis

Pyrolytic temperature for biochar synthesis can influence its carbonaceous structure as well as surface properties, which affect its adsorption and PDS activation performance directly. The effect of pyrolytic temperature for sludge biochar on PDS catalytic oxidation of TC was investigated, as illustrated in Fig. 2. The K_{app} values for the adsorption process alone by BC200, BC300, BC400, BC500 and BC600 are 8.22×10^{-4}, 3.85×10^{-4}, 9.82×10^{-4}, 1.62×10^{-3} and 6.01×10^{-3} min^{-1} ($R^2 = 0.917$, 0.917, 0.878, 0.828 and 0.885), respectively. As a comparison, the K_{app} values for the PDS cata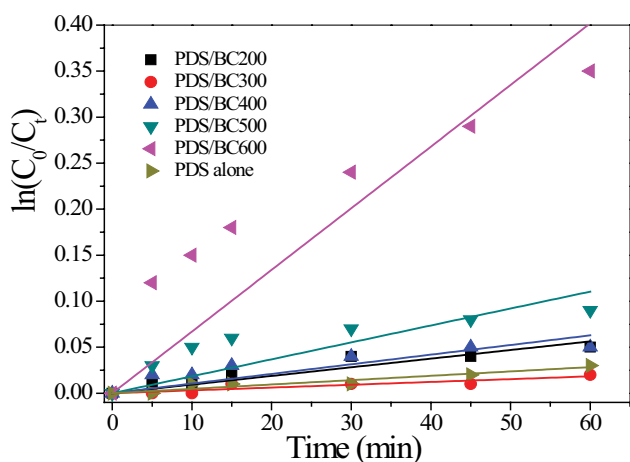lytic processes activated by BC200, BC300, BC400, BC500 and BC600 are of 9.38×10^{-4}, 3.05×10^{-4}, 1.05×10^{-3}, 1.84×10^{-3} and 1.24×10^{-2} min^{-1} ($R^2 = 0.954$, 0.902, 0.893, 0.862 and 0.972), respectively. Considering the synergetic effect occurring in the PDS catalytic process, the low-temperature biochars including BC200, BC300, BC400 and BC500 almost fail to activate the PDS oxidation process. Evidently, only the sludge biochar BC600 is capable of activating PDS for the catalytic degradation of TC. As high pyrolytic temperature is able to deactivate all oxygen-containing groups on a biochar, sludge biochars pyrolyzed at lower temperature usually have more abundant surface oxygen-containing functional groups. It can be deduced that the surface oxygen-containing functional groups is not the only parameters attributed to PDS activation. Further, as the pyrolytic temperature for biochar synthesis is usually selected at temperature lower than 600°C, the sludge biochar BC600 is applied in the following experiments.

3.2. Characterization of sludge biochar BC600 and ACO

3.2.1. Surface morphology

The surface morphologies and EDX results of the sludge biochar BC600 and ACO are presented in Fig. 3. It is observed that BC600 consists of particles with the diameters below 10 μm in our previous study [29]. The biochar flakes of BC600 have a loose and porous structure. By contrast, there are plenty of fine ACO carbon particles, while the strength of ACO is actually quite higher than that of BC600. The size of most of the ACO particle is within tens of nanometers. Concurrently, the atomic ratios of carbon and oxygen on sludge biochar BC600 were 54.9% and 29.5%, respectively, while they are 87.2% and 9.3% on ACO, respectively. Definitely, it is expected that the carbonaceous structure and surface properties of sludge biochar BC600

Fig. 2. Effect of pyrolytic temperature for sludge biochar synthesis on PDS catalytic oxidation of tetracycline.
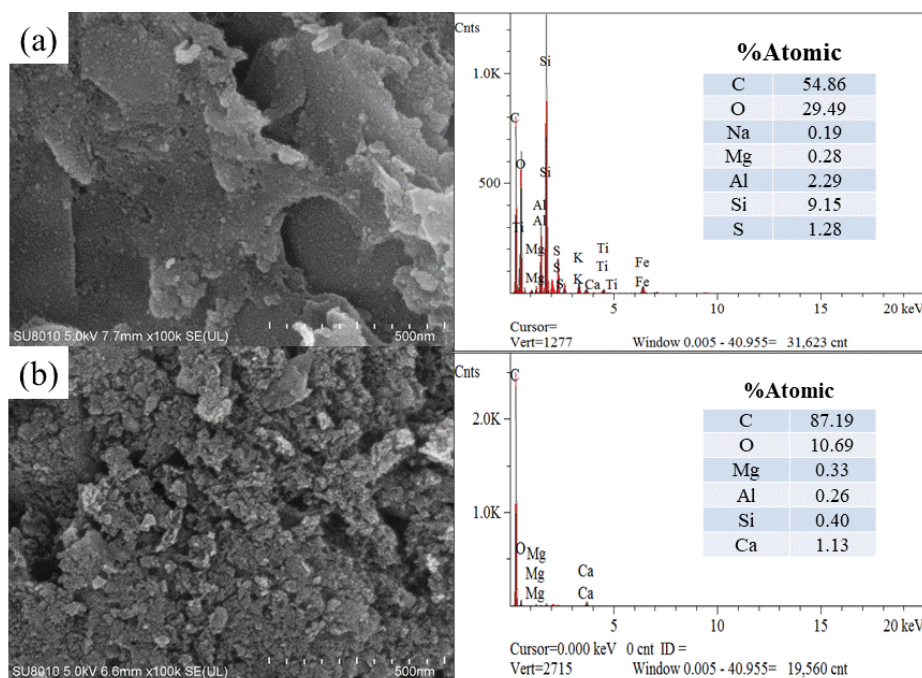

Fig. 3. Surface morphologies and energy-dispersive X-ray analysis results of (a) sludge biochar BC600 and (b) ACO.

and ACO might profoundly affect their PDS activation performance in the following experiments.

3.2.2. Fourier-transform infrared spectroscopy, X-ray diffraction, Raman and BET analysis

As carbonyl groups from aldehydes and ketones were considered to be able to activate PDS to generate singlet oxygen ($^1O_2$), one of the key oxidizing species for contaminants degradation [33,34], the effect of carbonyl groups on carbons should be figured out explicitly. As carboxylic acids, esters, amides and nitriles are more resistant towards $NaBH_4$, the reactivity of $NaBH_4$ can be enhanced in the presence of certain additives [35]. It is known that aldehydes and ketones can be reduced to alcohols with protic solvents. As such, in this case, both the raw and KBH_4-reduced carbons including BC600 and ACO are applied for activating PDS to explore the roles of carbonyl groups. As illustrated in Fig. 4a, the Fourier-transform infrared (FTIR) spectra of the raw and KBH_4-reduced BC600 or ACO were recorded. Typically, the four samples have several well-defined absorption bands indicating a certain amount of surface functional groups. Generally, the raw and KBH_4-reduced BC600 have more absorption bands including the bands at 790 and 1,613 cm^{-1} than those of the raw and KBH_4-reduced ACO. The strong band at 3,420 cm^{-1} represents the stretching vibration of adsorbed water. The four samples have a strong absorption band at 1,080 cm^{-1} (C–O stretching). The
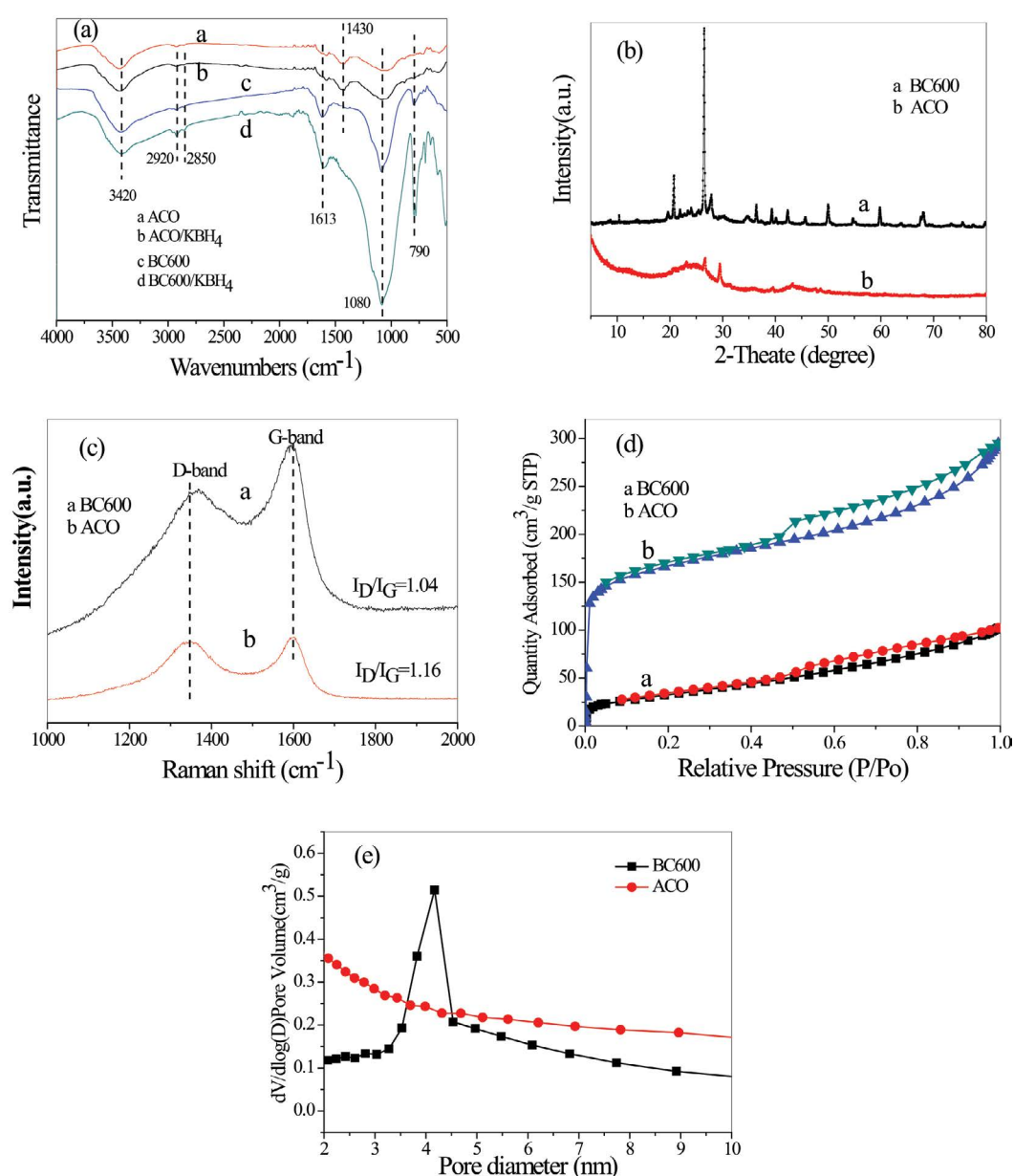

Fig. 4. Fourier-transform infrared spectra of the raw and KBH_4-reduced BC600 or ACO (a). X-ray diffraction patterns (b), Raman spectra (c), N_2 adsorption–desorption isotherms (d) and pore-size distribution (e) of BC600 and ACO.

bands at 2,920 and 2,850 cm^{-1} are assigned to aliphatic C–H stretching, while their intensities on the surface of both BC600 samples were stronger than those on both ACO samples. These indicate the significant loss of aliphatic C–H functional groups on ACO during industrial production. Meanwhile, the strong and well-defined band at around 1,613 cm^{-1} (aromatic C=C or C=O) is observed on the raw and KBH$_4$-reduced BC600 [36,37], reflecting more aromatic C=C or C=O groups on both BC600 samples. It should be mentioned that the band at 1,613 cm^{-1} shifts to 1,600 cm^{-1} on the KBH$_4$-reduced BC600, indicating the effect of KBH$_4$ by reducing C=O to C–OH. Additionally, the band at around 1,430 cm^{-1} (aromatic C=C) is only present on the raw and KBH$_4$-reduced ACO, which corresponds to the high carbon content of ACO. Interestingly, new bands at 580, 649 and 690 cm^{-1} emerged on the reduced BC600 as well. Accordingly, these emerging C–H structures are generated as a result of the BC600 reduction by KBH$_4$. As such, both the raw and KBH$_4$-reduced BC600 have more abundant surface oxygen-containing groups than the raw and KBH$_4$-reduced ACO. This is consistent with the higher atomic ratio of oxygen on BC600 than on ACO by EDX analysis. These indicate the four carbonaceous samples possessed quite different surface properties especially for functional groups.

Evidently, Fig. 4b indicates that the X-ray diffraction patterns of BC600 are well-defined while those of fine ACO particles are particularly broader. As the prepared biochars contains a certain amount of minerals, the diffraction peaks on BC600 are abundant and more well-defined [38]. Two diffraction peaks around $2\theta \approx 23°$ and $44°$ on ACO are characteristic of the C (002) and C (101) diffractions, reflecting the disordered graphitic planes of non-crystalline and crystalline/graphitic (sp^2-hybridized) carbon, respectively [39]. This demonstrates a more disordered graphitic structure on ACO. Meanwhile, the distinct peak at 25.9° corresponding to the (002) facet of graphite is observed apparently lower on ACO than on BC600, which demonstrates that a higher graphitic defect existent on ACO than on BC600. From Fig. 4c, the spectra of both carbons present two bands at ca. 1,346 and 1,599 cm^{-1}, corresponding to the characteristic D and G bands (disordered and sp^2-ordered C structures), respectively. The ratio of the intensity of the two peaks, I_D/I_G, for BC600 and ACO are found to be 1.04 and 1.16, respectively, indicating that ACO has more defect sites in its carbon structure than BC600.

As shown in Fig. 4d and e, the specific surface area and pore-size distributions of BC600 and ACO are compared through nitrogen adsorption–desorption isotherms. Typically, the curves displayed type IV isotherms and H$_4$ hysteresis loop, indicating the presence of micropores and mesopores within both carbonaceous materials [40]. Both BC600 and ACO have hierarchical pore structures. The pore size of BC600 is centered at 4.18 nm while ACO has a comparatively uniform distribution. The distinct surface characteristic and functional groups of BC600 and ACO are also listed in Table 1. The average pore size of BC600 and ACO achieved 5.23 and 4.64 nm, respectively. The surface functional groups of BC600 and ACO were quantitatively measured by Boehm's titration method. The total content of carboxyl, lactonic, phenolic groups and carbonyl group on BC600 were of 1.06, 0.315, 0.138 and 1.66 mmol·g^{-1}, respectively, while 0.67, 0.067, 0.079 and 2.22 mmol·g^{-1} on ACO, respectively. Totally, ACO is characterized with larger surface area/pore volume and higher carbon content. By contrast, BC600 has a particularly higher content of oxygen and surface oxygen-containing groups including carboxyl, lactonic, and phenolic groups. As such, the PDS activation performance of BC600 and ACO might differ significantly from this point of view.

Concerning the chemical nature of surface functional groups, the X-ray photoelectron (XPS) spectra of O1s, C1s and wide scan XPS spectra of the BC600 and ACO are measured and presented in Fig. 5. As illustrated in Fig. 5a, BC600 and ACO have similar wide scan XPS spectra of carbonaceous structure. From Fig. 5b, it is noted that the O1s intensity of BC600 is apparently higher than that of ACO, indicating a higher O content on BC600 as well. Concurrently, the asymmetric C1s XPS patterns in Fig. 5c for the two carbons are quantitatively differentiated into four different carbon stages, including the sp^2 hybridized carbon (284.6 eV), the alcohol/ether group (C–O, about 286.2 eV), carbonyl group (C=O, about 287.4 eV) and carboxyl acid/ester group (O–C=O, about 288.7 eV) [41,42]. The peak at 285.5 eV was attributed to defective carbon on ACO structure [43], indicating the abundant carbon defects on ACO (10.9%) other than on BC600. From Fig. 5d and e, it is evident that BC600 has abundant C–O and O–C=O groups on their surface while ACO is lack of these functional groups. The chemical state distribution shows that the total proportion of C=O, C–O and O–C=O groups is 32.4% on BC600 while those on ACO is 9.3%, which is consistent with the Boehm's titration result. Both C–O and O–C=O groups are associated with strong electron-donating group, while C=O group with electron-withdrawing effect. As such, it is difficult to speculate the roles of these functional groups of carbon on TC adsorption and oxidation.

3.3. Synergy and effect of carbon dose on the degradation of TC

Based on the structure and surface property disparity between BC600 and ACO, their PDS catalytic performance is expected to be quite different, as illustrated in Fig. 6a. On one hand, the K_{app} values for ACO and BC600 adsorption

Table 1
Surface characteristics and functional groups of BC600 and ACO

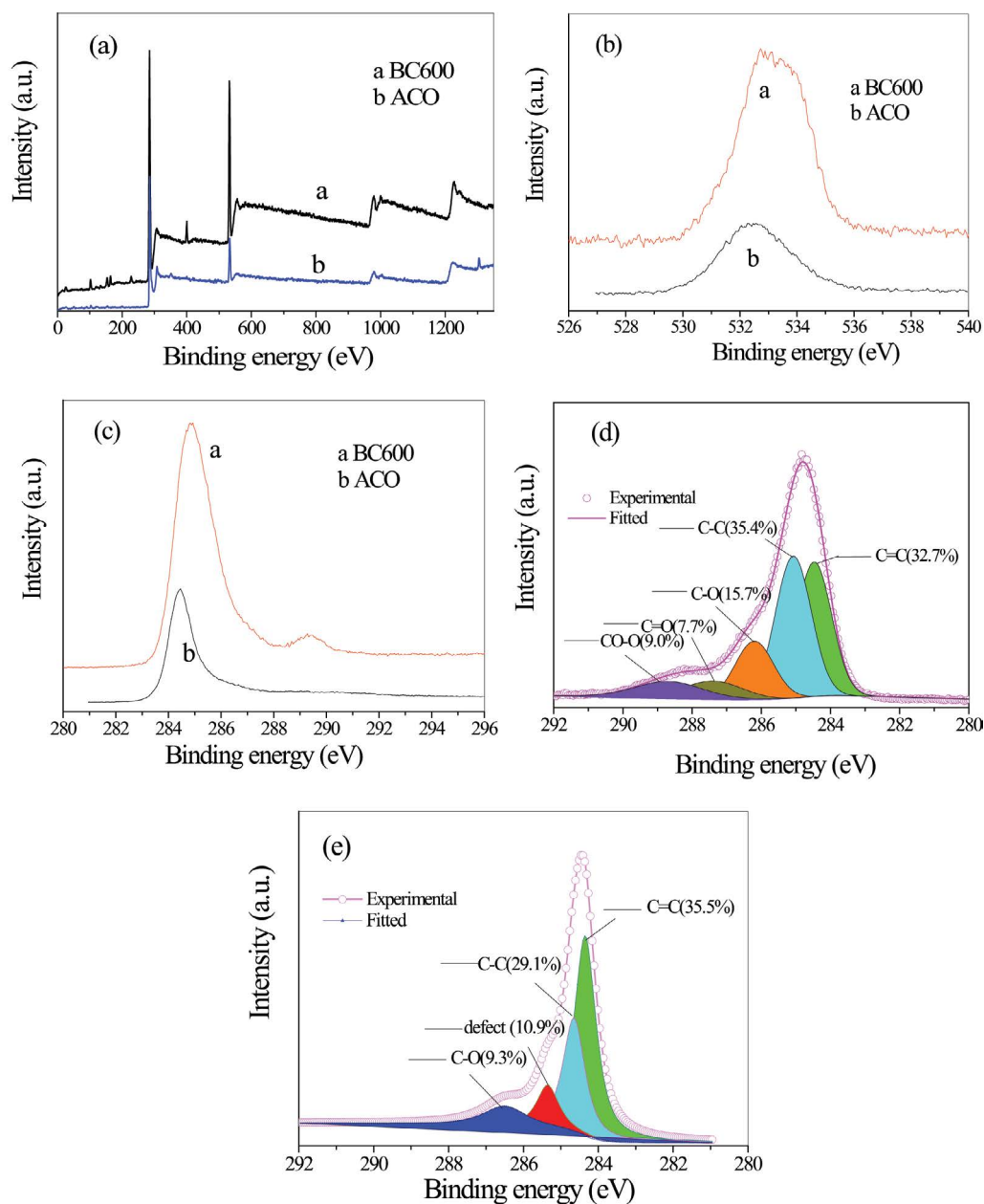|	BC600	ACO
C%	54.9	87.2
O%	29.5	9.3
Specific surface area (m^2·g^{-1})	119.0	554.2
Pore volume (cm^3·g^{-1})	0.155	0.449
Average pore size (nm)	5.23	4.64
Carboxyl (mmol·g^{-1})	1.06	0.67
Lactonic group (mmol·g^{-1})	0.315	0.067
Phenolic group (mmol·g^{-1})	0.138	0.079
Carbonyl (mmol·g^{-1})	1.66	2.22

Fig. 5. High-resolution X-ray photoelectron spectra of BC600 and ACO. (a) Wide scan X-ray photoelectron spectra, (b) O1s, (c) C1s, and (d) C1s mapping of BC600 and (e) C1s mapping of ACO.

are 1.04×10^{-2} and 6.01×10^{-3} min^{-1} (R^2 = 0.897 and 0.895), respectively. EDX analysis indicates atomic ratios of oxygen on BC600 and ACO are 29.5% and 10.7%, respectively. Although the content of surface oxygen-containing functional groups on BC600 is dramatically higher than those of ACO, its adsorption capability for TC is evidently lower than that of ACO. On the other hand, the K_{app} values for the combined BC600-PDS and ACO-PDS process are 1.24×10^{-2} and 2.50×10^{-2} min^{-1} (R^2 = 0.972 and 0.945), respectively. The K_{app} value for the combined ACO-PDS process was 2.15 times that of the sum of K_{app} values of the other two processes, while it was 1.72 times for the BC600-PDS process. The total organic carbon removal efficiency by BC600-PDS and

ACO-PDS processes achieve 33.1% and 38.0%, respectively. These indicate that both ACO and BC600 have generated synergetic effect while ACO seems to be a more powerful carbon catalyst for PDS activation. By contrast, the K_{app} values for the combined KBH$_4$-reduced BC600-PDS and KBH$_4$-reduced ACO-PDS process are 9.8×10^{-3} and 2.59×10^{-2} min^{-1} (R^2 = 0.921 and 0.938), respectively. The reduction of carbonyl group actually declines the capability of BC600 of activating PDS. However, the reduction of carbonyl group almost does not affect the PDS catalytic performance of ACO.

It was reported that the intrinsic and external characteristics of carbonaceous materials, including dimensionality, pristine carbon configuration, crystallinity and defects,
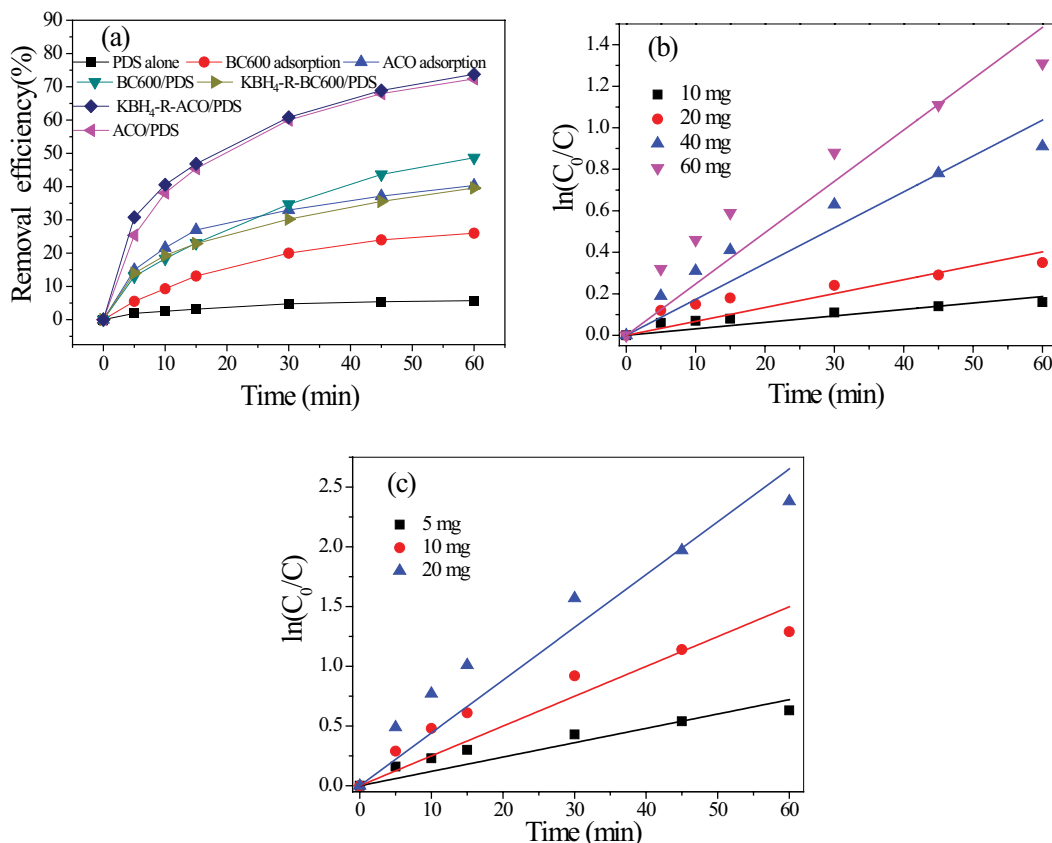
Fig. 6. Synergetic degradation of tetracycline. Carbon 10 mg, PDS 30 mg·L^{-1} (a) and carbon dose effect for the PDS catalytic process by BC600 (b) and ACO (c).

porosity, chemical active groups, and heterogeneous doping, affect the persulfate activation and thus the degradation of organic pollutants [44]. Typically, the surface areas of ACO and BC600 are 554.2 and 119.0 m²·g^{-1}, respectively, while their average pore sizes are 5.23 and 4.64 nm, respectively. Considering the insignificant effect of surface oxygen-containing functional groups and carbonyl group revealed above, it is quite reasonable to deduce that crystallinity and defects have played a critical role for activating PDS. Point defects include edges, vacancies, oxygen functional groups, and merged foreign atoms [45]. As mentioned above, the abundant carbon defects on ACO (10.9%) is observed on ACO other than on BC600, which is consistent with the Raman analysis results. Meanwhile, more oxygen functional groups on BC600 might have occupied its existing defects and inhibit PDS activation via steric hindrance [45]. It was discovered that the delocalized electrons from these defects could activate persulfate, resulting in the scission of O−O bonds and the formation of reactive radicals [44]. Accordingly, it is expected that surface defects on both carbon have contributed to the activation of PDS and degradation of TC.

Further, from Fig. 6b and c, the K_{app} values for the BC600 dose at 10, 20, 40 and 60 mg are 3.11×10^{-3}, 6.70×10^{-3}, 1.73×10^{-2} and 2.47×10^{-2} min^{-1} (R^2 = 0.910, 0.912, 0.956 and 0.952), respectively. As a comparison, the K_{app} values for the ACO dose at 5, 10 and 20 mg are 1.20×10^{-2}, 2.50×10^{-2} and 4.42×10^{-2} min^{-1} (R^2 = 0.945, 0.946 and 0.963), respectively.

Therefore, the efficiency of BC600 dose at 60 mg is equivalent to that of ACO at 10 mg. ACO is therefore proved to be quite superior to BC600 concerning the PDS catalytic degradation process. Considering the effect of adsorption, the dose of BC600 and ACO was selected to be 20 and 10 mg, respectively in the following experiments.

3.4. Effect of PDS dose and solution pH

The effect of PDS dose and solution pH on the degradation of TC was also investigated, as depicted in Fig. S1. From Fig. S1a it can be observed that an increase in PDS dose from 10 to 30 mg·L^{-1} could result in an increasing removal efficiency of TC. However, for both BC600 and ACO, the removal efficiencies at PDS dose of 3 and 6 mg had no significant difference, which implied that there was an optimal PDS dose for the degradation process. As the limited amount of active sites could activate the equivalent amount of PDS, the excessive amount of PDS might decompose by oxidizing the carbon catalyst. Meanwhile, solution pH could influence the surface properties of carbon as well as the distribution species of TC. As presented in Fig. S1b and c, the initial solution pH dramatically affected the PDS degradation efficiency on both BC600 and ACO, although the extent on BC600 was evidently higher than that on ACO. Generally, the lower the initial solution pH, the higher the degradation efficiency was achieved. The adsorption of TC

onto the carbonaceous materials is the first step for subsequent PDS degradation. Accordingly, the zeta potential of carbon surface was measured at neutral solution and illustrated in Fig. S1d and the zeta potential values of BC600 and ACO were located at –15.00 and –9.29 mV, respectively. It indicates that both BC600 and ACO become more positively-charged in acidic solution while more negatively-charged in alkaline solution. As TC (H_2L) is an amphoteric compound with pKa values at 3.3, 7.7, and 9.7, its predominant species are deduced to be cation at pH < 3.3, zwitterions at 3.3 < pH < 7.7, and negatively charged anions at pH > 7.7. As such, it can be estimated that neutral solution pH is favorable for TC uptake while the adsorption of TC is highly inhibited under acidic and alkaline conditions as a result of the repulsive force between carbons and TC molecules. The comparatively higher PDS degradation efficiency at solution pH 5 and 7 actually proved the role of TC uptake on the total degradation process. Eventually, the zeta potential of BC600 and ACO is quite similar, which might not be the key factor determining the degradation performance.

3.5. Predominant roles of oxidizing species

3.5.1. Roles of OH radicals and sulfate radicals

Concerning the roles of OH radicals and sulfate radicals, methanol (MeOH) and tert-butyl alcohol (TBA) were usually used to quench these radicals and get some new information [46,47]. MeOH with α-H reacts immediately with $OH^\bullet$ and $SO_4^{\bullet-}$ under nearly the same rate ($k_{OH^\bullet}$ = 1.2 × 10^9 – 2.8 × 10^9 M$^{-1}\cdot$s^{-1}, $k_{SO_4^\bullet}$ = 1.6 × 10^7 – 7.7 × 10^7 M$^{-1}\cdot$s^{-1}), while TBA without α-H presents three orders of magnitude higher reaction rates with $OH^\bullet$ and $SO_4^{\bullet-}$ ($k_{OH^\bullet}$ = 6.0 × 10^8 M$^{-1}\cdot$s^{-1}, $k_{SO_4^\bullet}$ = 4.0 × 10^5 M$^{-1}\cdot$s^{-1}). As presented in Fig. S2, the inhibitory effect caused by both MeOH and TBA was no so significant on both BC600 and ACO. It should be mentioned that the quenching effect was also not pronounced on both reduced BC600 and ACO. For example, the K_{app} values for the raw BC600 declined from 1.24 × 10^{-2} min^{-1} (R^2 = 0.972) without MeOH to 9.42 × 10^{-3} min^{-1} (R^2 = 0.972) with MeOH (MeOH:PDS = 100:1). Comparatively speaking, this quenching effect was slightly more evident on BC600, although a significant drop of degradation efficiency was not observed. As such, the contribution of both $OH^\bullet$ and $SO_4^{\bullet-}$ was almost negligible compared to the overall degradation efficiency.

3.5.2. Roles of superoxide radical, singlet oxygen and active holes

As a series of oxidizing species are involved in the PDS catalytic process, p-benzoquinone (Bq), NaN$_3$ and EDTA-2Na (EDTA) were employed to probe the existence of superoxide radical ($O_2^{\bullet-}$), singlet oxygen ($^1O_2$) and active holes (h$^+$), respectively [21,48–50]. As illustrated in Fig. S3, for both BC600 and ACO, the three scavengers were evidently capable of inhibiting the reaction to different extents. Superoxide radicals were inhibited significantly by Bq on both carbons, as illustrated in Fig. S3a and b. In the presence of 3.8 mM of

Bq, the K_{app} values for the raw BC600 and ACO declined to 4.36 × 10^{-3} min^{-1} (R^2 = 0.906) and 8.55 × 10^{-3} min^{-1} (R^2 = 0.904), respectively. The contribution K_{app} for BC600 and ACO achieved 8.05 × 10^{-3} min^{-1} and 1.85 × 10^{-2} min^{-1}, respectively. Accordingly, the contribution percentage of $O_2^{\bullet-}$ for BC600 and ACO was 64.9% and 68.3%, respectively. Second, from Fig. S3c and d, as to NaN$_3$, the K_{app} values for the raw BC600 declined from 1.24 × 10^{-2} min^{-1} (R^2 = 0.972) without NaN$_3$ to 7.71 × 10^{-3} min^{-1} (R^2 = 0.918) with NaN$_3$ (0.02 mol·L^{-1}), while the K_{app} values for the raw ACO declined from 2.70 × 10^{-2} min^{-1} (R^2 = 0.942) without NaN$_3$ to 1.11 × 10^{-2} min^{-1} (R^2 = 0. 891) with NaN$_3$ (0.02 mol·L^{-1}). The contribution K_{app} for BC600 and ACO achieved 4.69 × 10^{-3} min^{-1} and 1.59 × 10^{-2} min^{-1}, respectively. Accordingly, the contribution percentage of singlet $^1O_2$ for BC600 and ACO was 37.8% and 58.9%, respectively. Finally, from Fig. S3e and f, active holes were efficiently captured by EDTA. In the presence of 0.10 g·L^{-1} of EDTA-2Na, the K_{app} values for the raw BC600 and ACO declined to 7.38 × 10^{-3} min^{-1} (R^2 = 0.964) and 1.11 × 10^{-2} min^{-1} (R^2 = 0.945), respectively. The contribution K_{app} for BC600 and ACO achieved 5.03 × 10^{-3} min^{-1} and 1.59 × 10^{-2} min^{-1}, respectively. Accordingly, the contribution percentage of h$^+$ for BC600 and ACO was 40.5% and 58.7%, respectively. Totally, the contribution percentage of $O_2^{\bullet-}$ was very close on both carbons, while those of $^1O_2$ and h$^+$ on ACO achieved about 50% higher than those on BC600.

3.6. Effect of surface oxygen-containing functional groups

Concerning generation of active holes, Radovic et al. [51] reported that the addition of carboxyl groups (electron-withdrawing) at the edges of the individual graphene layers within activated carbons (ACs) causes a considerable drop in the ACs p-electron density, while positive holes are consequently created in the conduction p-band of the individual graphene layers. Similarly, the generation of active holes on BC600 and ACO are deduced to be highly dependent on the existing carboxyl groups. From Table 1 the contents of carboxyl, lactonic and phenolic groups on BC600 are all higher than those on ACO. The content of carboxyl groups on BC600 and ACO are respectively 1.06 and 0.67 mmol·g^{-1}, and more active holes are expected to be generated on BC600 than on ACO. However, about 50% more h$^+$ was generated on ACO than on BC600. As such, it is difficult to confirm the activation effect of carboxyl groups on both carbons.

Further, some researchers reported that carbonyl groups were responsible for the generation of singlet oxygen while carbonyl groups are the main active site for PDS catalysis [52,53]. As we know, carbonyl groups can be well reduced by KBH$_4$ in absolute alcohol, and the surface properties of both BC600 and ACO were altered consequently. Effect of KBH$_4$-reduction on BC600 and ACO for TC degradation was investigated, as illustrated in Fig. 7. Concerning the adsorption process alone, as shown in Fig. 7a and b, the K_{app} values for the raw BC600, raw ACO, reduced BC600 and reduced ACO were 6.01 × 10^{-3} min^{-1} (R^2 = 0.895), 1.04 × 10^{-2} min^{-1} (R^2 = 0.897), 7.43 × 10^{-3} min^{-1} (R^2 = 0.909), and 1.27 × 10^{-2} min^{-1} (R^2 = 0.893), respectively. It means that the adsorption capability of the reduced BC600 and ACO was improved after KBH$_4$-reduction in absolute

alcohol. Absolute alcohol could extract organics from the two carbons, which might be attributed to the enhanced adsorption sites and improved adsorption performance. Second, as to the PDS catalytic process, the K_{app} value for the reduced BC600 declined slightly compared to the raw BC600, while the value for the reduced ACO increased insignificantly in comparison with the raw ACO. The content of carbonyl groups on BC600 and ACO are measured to be 1.66 and 2.22 mmol·g^{-1}, respectively. It was actually speculated that the K_{app} value for the reduced ACO declined more significantly compared with that of the reduced BC600. So, it is impossible to verify the predominant role of carbonyl groups in carbon-catalyzed PDS oxidation process. As such, the surface functional groups including carboxyl, carbonyl, lactonic and phenolic groups did not contribute to the activation of PDS in this case evidently.

Meanwhile, the contribution percentages of superoxide radicals ($O_2^{\bullet-}$), $^1O_2$ and active holes (h$^+$) for the two reduced carbons are also presented in Fig. 7c. Typically, the contribution percentages of $^1O_2$ and h$^+$ were almost not affected by KBH$_4$-reduction on both BC600 and ACO. This result is distinctive as documents confirmed that carbonyl groups were mainly responsible for the generation of $^1O_2$, one of the key oxidizing species in the non-radical PDS catalytic degradation process. By contrast, the contribution percentage of $O_2^{\bullet-}$ on the raw BC600, reduced BC600, raw ACO and reduced ACO achieved 64.9%, 44.6%, 68.3% and 60.5%, respectively. This demonstrated that the generation

of $O_2^{\bullet-}$ was evidently suppressed on the reduced BC600 but insignificantly on the ACO, indicating the limited role of carbonyl groups on the generation of $O_2^{\bullet-}$. On the other hand, it also indicated that carbonyl groups might be responsible for generating $O_2^{\bullet-}$ on carbon/water interface to some extent. From this point of view, the effect of carbonyl groups on PDS catalytic process was quite limited to some extent.

The defect structures of carbonaceous materials including biochars were considered to be quite associated with the activation of PDS for contaminants degradation [54–56]. The concrete relationship between defects/inorganic component and oxidation mechanisms by $O_2^{\bullet-}$ and $^1O_2$ was confirmed during swine bone biochar-activating PDS oxidation process, in which the role of $O_2^{\bullet-}$ and $^1O_2$ was consolidated accordingly. As mentioned above, the ratio of I_D/I_G for BC600 and ACO were 1.04 and 1.16, respectively, while their specific surface area achieved 119.0 and 554.2 m^2·g^{-1}, respectively. It can be reasonably deduced that the amount of defect structures on ACO is about 5 times that on BC600. As such, considering the especially higher surface area of ACO than BC600, the defect structures including edge defects, curvatures and vacancies are more abundant on ACO than on BC600 [57]. These defect structures can generate dangling σ bonds, which facilitates the edge carbons to donate delocalized π-electrons and activate PDS for fast tetracycline degradation. As such, the defects on both carbons have played the key role for the PDS catalytic process as presented below:
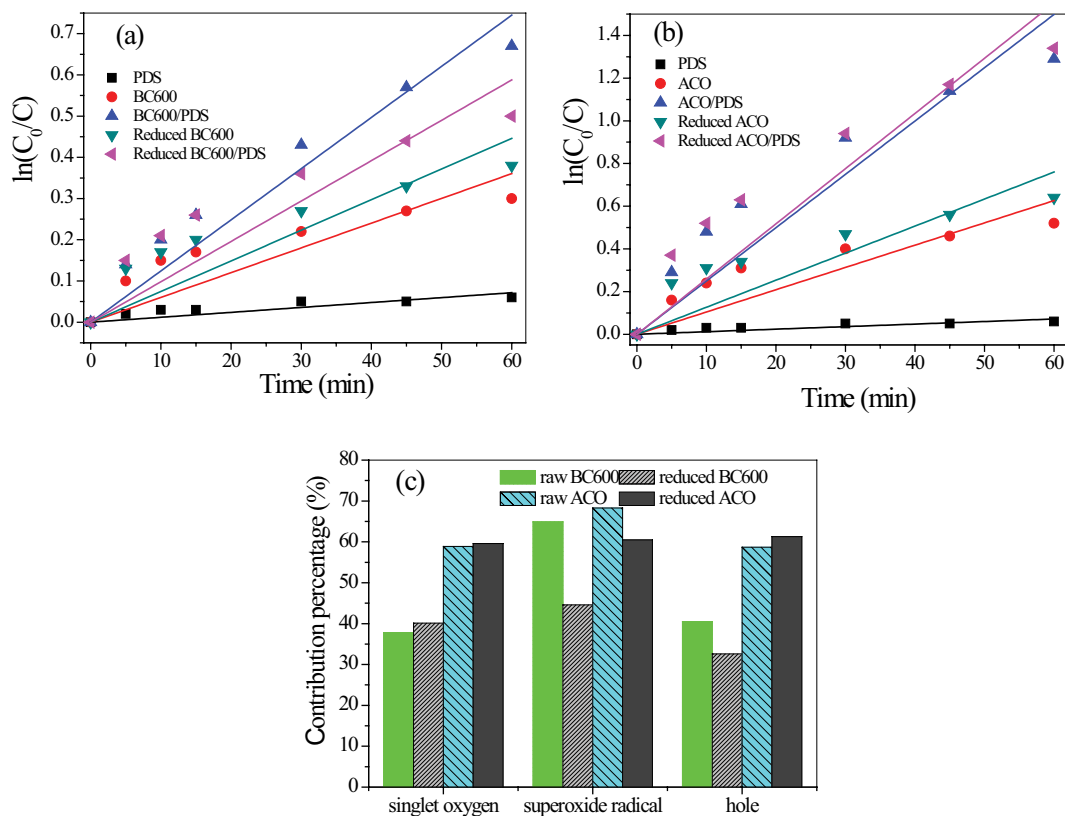

Fig. 7. Effect of carbonyl groups on tetracycline degradation. BC600 (a), ACO (b) and contribution percentages of various oxidizing species involved (c).
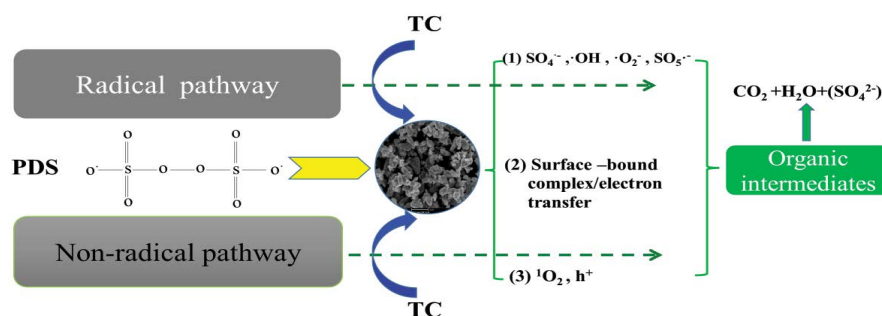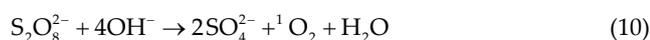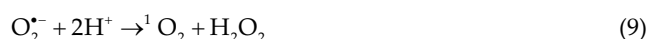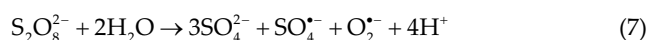
Fig. 8. Mechanism for degradation of tetracycline by carbon/PDS catalytic process.

$$HSO_5^- + C_{defects} \rightarrow OH^- + SO_4^{\bullet-} + C_{defects^+} \tag{4}$$

$$HSO_5^- + C_{defects} \rightarrow OH\cdot + SO_4^{2-} + C_{defects^+} \tag{5}$$

$$HSO_5^- + SO_4^{\bullet-} \rightarrow HSO_4^- + SO_5^{\bullet-} \tag{6}$$

$$S_2O_8^{2-} + 2H_2O \rightarrow 3SO_4^{2-} + SO_4^{\bullet-} + O_2^{\bullet-} + 4H^+ \tag{7}$$

$$SO_4^{\bullet-} + H_2O \rightarrow SO_4^{2-} + H^+ + OH^\bullet \tag{8}$$

$$O_2^{\bullet-} + 2H^+ \rightarrow {}^1O_2 + H_2O_2 \tag{9}$$

$$S_2O_8^{2-} + 4OH^- \rightarrow 2SO_4^{2-} + {}^1O_2 + H_2O \tag{10}$$
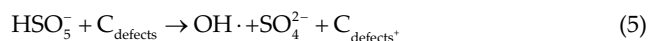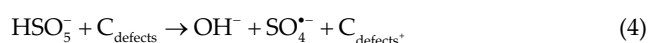
Additionally, a series of radical and non-radical oxidizing species are generated when PDS was catalyzed by both carbons, according to Eqs. (4)–(6). In this case, ${}^1O_2$, $O_2^{\bullet-}$ and h^+ are confirmed to be the key oxidizing species for tetracycline. As far as the oxidizing species are concerned, the oxidation potential of ${}^1O_2$ and $O_2^{\bullet-}$ are E^0 (${}^1O_2/O_2$) = 1.88 V and E^0 ($O_2^{\bullet-}/H_2O$) = 2.6 V, respectively. As presented in Eq. (9), ${}^1O_2$ can be directly transformed from $O_2^{\bullet-}$ in this approach. As the oxidizing capability of $O_2^{\bullet-}$ is much higher than that of ${}^1O_2$, the consumption of $O_2^{\bullet-}$ by organic contaminants could lead to a very limited amount of ${}^1O_2$. Accordingly, it is expected that the amount of $O_2^{\bullet-}$ measured by quenching was much higher than that of ${}^1O_2$. This is why the contribution percentage of $O_2^{\bullet-}$ was higher than that of ${}^1O_2$ on both carbons as illustrated in Fig. 7c.

It will always fall into discrepancy when discussing PDS activation and oxidation mechanism as the dominant oxidizing species mainly vary with target contaminants, catalyst composition and structure involved. One important thing we should consider is that adsorption of both TC and PDS molecules is prerequisite of catalytic process as most of the reactions occur in the vicinity of water/carbon interfaces other than in the bulk solution. Concerning BC600 and ACO, the reaction mechanism for TC degradation is presented in Fig. 8. As to metal-free/carbonaceous catalysts, PDS activation usually undergoes a complex oxidation mechanism. First, in the radical pathway, a number of free radicals including $OH^\bullet$, $SO_4^{\bullet-}$ and $O_2^{\bullet-}$ are generated in the catalytic process. They have strong oxidizing capability while their generation amount is quite insignificant judged

from Fig. S2. Considering the short lifetime of these free radicals, radical oxidation is limited within the water/carbon interfaces, while their efficiency might be prevailing if sufficient radicals were captured by the TC molecules adsorbed by carbonaceous surface/pores. In this case, $O_2^{\bullet-}$ had actually played a quite important role. Second, non-radical pathway proved to be dominant in most of the carbon-involved PDS catalytic process. Oxidizing species such as ${}^1O_2$ and active holes were concurrently generated directly on carbon surface or indirectly from radical pathway. Fig. S3 demonstrates substantial generation of ${}^1O_2$ and active holes in this research, indicating the predominant role of non-radical species. Finally, and most important, one important fact is that no one scavenger have quenched the PDS activation and oxidation process completely. In parallel to the radical and non-radical pathway, electron transfer mechanism was confirmed by the effect and role surface-bound complexes (carbon-PDS*) [21–23]. From this point of view, the surface-bound complexes are quite stable when confronted with these various scavengers. Totally, the PDS activation and oxidation process is a quite complicated process involving different approaches and mechanisms.

3.7. Reusability of both carbons

In order to verify the reusability and stability of the two carbons in the PDS catalytic process, repeated use experiment was conducted. In a run, after 60 min of reaction duration, the solution was precipitated and supernatant was drawn. Then, 100 mL of new TC solution (10 mg·L^{-1}) was added in the flask to continue the PDS catalytic process. As such, an obvious loss of carbons was observed when decanting the supernatant. Even though, as presented in Fig. S4, there still remained a certain degradation capability for both carbons after four run of catalytic process. Comparatively speaking, ACO performed better for the removal of TC than BC600. Particularly, the fourth reuse by ACO still maintains a removal rate of 47.4%, while the initial use of ACO achieves 72.4% of removal. In a word, the recycled carbons can be applied for repeated use for PDS catalytic degradation of TC, and ACO proves to be a suitable carbon applied in practical water and wastewater treatment.

4. Conclusion

As meso-porous materials, sludge biochar BC600 and ACO proved to be capable of catalyzing PDS oxidation of

tetracycline. BC600 is of low carbon content and abundant surface oxygen-containing functional groups, while ACO has high carbon content and less surface functional groups. However, ACO demonstrates an especially higher PDS activation capability than BC600. Solution pH had a more dramatic influence on BC600 compared with ACO. Quenching experiments indicated that both $OH^\bullet$ and $SO_4^{\bullet-}$ contributed insignificantly while most of the TC degradation was attributed to superoxide radical ($O_2^{\bullet-}$), singlet oxygen ($^1O_2$) and active holes (h^+). Both the untreated and KBH_4-reduced carbons are employed to explore the roles of carbonyl groups, while quenching experiments did not indicate the key role of carbonyl groups for $^1O_2$ generation. In terms of degradation mechanism, radical pathway and non-radical pathway are all involved for the carbon/PDS catalytic process. Excellent reusability and stability of ACO was observed in repeated use experiment.

Acknowledgements

References

[1] D. Belkheiri, F. Fourcade, F. Geneste, D. Floner, H. Aït-Amar, A. Amrane, Combined process for removal of tetracycline antibiotic – coupling pre-treatment with a nickel-modified graphite felt electrode and a biological treatment, Int. Biodeterior. Biodegrad., 103 (2015) 147–153.

[2] L.B. Zhang, S.Y. Shen, Adsorption and catalytic degradation of sulfamethazine by mesoporous carbon loaded nano zero valent iron, J. Ind. Eng. Chem., 83 (2020) 123–135.

[3] L. Tang, Y.N. Liu, J.J. Wang, G.M. Zeng, Y.C. Deng, H.R. Dong, H.P. Feng, J.J. Wang, B. Peng, Enhanced activation process of persulfate by mesoporous carbon for degradation of aqueous organic pollutants: electron transfer mechanism, Appl. Catal., B, 231 (2018) 1–10.

[4] J.L. Wang, R. Zhuan, Degradation of antibiotics by advanced oxidation processes: an overview, Sci. Total Environ., 701 (2020) 135023, doi: 10.1016/j.scitotenv.2019.135023.

[5] R. Anjali, S. Shanthakumar, Insights on the current status of occurrence and removal of antibiotics in wastewater by advanced oxidation processes, J. Environ. Manage., 246 (2019) 51–62.

[6] T. Zhang, Y. Chen, Y. Wang, J. Le Roux, Y. Yang, J. Croué, Efficient peroxydisulfate activation process not relying on sulfate radical generation for water pollutant degradation, Environ. Sci. Technol., 48 (2014) 5868–5875.

[7] X.G. Duan, Z.M. Ao, H.Y. Zhang, M. Saunders, H.Q. Sun, Z.P. Shao, S.B. Wang, Nanodiamonds in sp^2/sp^3 configuration for radical to non-radical oxidation: core-shell layer dependence, Appl. Catal., B, 222 (2018) 176–181.

[8] M. Golshan, B. Kakavandi, M. Ahmadi, M. Azizi, Photocatalytic activation of peroxymonosulfate by TiO_2 anchored on cupper ferrite ($TiO_2@CuFe_2O_4$) into 2,4-D degradation: process feasibility, mechanism and pathway, J. Hazard. Mater., 359 (2018) 325–337.

[9] A. Ghauch, A.M. Tuqan, N. Kibbi, Ibuprofen removal by heated persulfate in aqueous solution: a kinetics study, Chem. Eng. J., 197 (2012) 483–492.

[10] C.S. Zhou, J.W. Wu, L.L. Dong, B.F. Liu, D.F. Xing, S.S. Yang, X.K. Wu, Q. Wang, J.N. Fan, L.P. Feng, G.L. Cao, Removal of antibiotic resistant bacteria and antibiotic resistance genes in wastewater effluent by UV-activated persulfate, J. Hazard. Mater., 388 (2020) 122070, doi: 10.1016/j.jhazmat.2020.122070.

[11] Y. Liu, Y. Zhang, A. Zhou, M. Li, Insights into carbon isotope fractionation on trichloroethene degradation in base activated persulfate process: the role of multiple reactive oxygen species, Sci. Total Environ., 800 (2021) 149371, doi: 10.1016/j.scitotenv.2021.149371.

[12] S.L. Wang, N. Zhou, Removal of carbamazepine from aqueous solution using sono-activated persulfate process, Ultrason. Sonochem., 29 (2016) 156–162.

[13] X.Y. Xu, J.Y. Qin, Y. Wei, S.C. Ye, J. Shen, Y. Yao, B. Ding, Y.R. Shu, G.Y. He, H.Q. Chen, Heterogeneous activation of persulfate by $NiFe_{2-x}Co_xO_4$-RGO for oxidative degradation of bisphenol a in water, Chem. Eng. J., 365 (2019) 259–269.

[14] B. Kakavandi, S. Alavi, F. Ghanbari, M. Ahmadi, Bisphenol a degradation by peroxymonosulfate photo-activation coupled with carbon-based cobalt ferrite nanocomposite: performance, upgrading synergy and mechanistic pathway, Chemosphere, 287 (2022) 132024, doi: 10.1016/j.chemosphere.2021.132024.

[15] Z. Liu, H. Ding, C. Zhao, T. Wang, P. Wang, D.D. Dionysiou, Electrochemical activation of peroxymonosulfate with ACF cathode: kinetics, influencing factors, mechanism, and application potential, Water Res., 159 (2019) 111–121.

[16] X. Sun, Z. Liu, Z. Sun, Electro-enhanced degradation of atrazine via Co-Fe oxide modified graphite felt composite cathode for persulfate activation, Chem. Eng. J., 433 (2022) 133789, doi: 10.1016/j.cej.2021.133789.

[17] X.G. Duan, H.Q. Sun, Z.P. Shao, S.B. Wang, Non-radical reactions in environmental remediation processes: uncertainty and challenges, Appl. Catal., B, 224 (2018) 973–982.

[18] Y.K. Fu, L. Qin, D.L. Huang, G.M. Zeng, C. Lai, B.S. Li, J.F. He, H. Yi, M.M. Zhang, M. Cheng, X.F. Wen, Chitosan functionalized activated coke for Au nanoparticles anchoring: green synthesis and catalytic activities in hydrogenation of nitrophenols and azo dyes, Appl. Catal., B, 255 (2019) 117740, doi: 10.1016/j.apcatb.2019.05.042.

[19] H.Q. Sun, S.Z. Liu, G.L. Zhou, H.M. Ang, M.O. Tadé, S.B. Wang, Reduced graphene oxide for catalytic oxidation of aqueous organic pollutants, ACS Appl. Mater. Interfaces, 4 (2012) 5466–5471.

[20] H.Z. Wang, W.Q. Guo, B.H. Liu, Q.L. Wu, H.C. Luo, Q. Zhao, Q.S. Si, F. Sseguya, N.Q. Ren, Edge-nitrogenated biochar for efficient peroxydisulfate activation: an electron transfer mechanism, Water Res., 160 (2019) 405–414.

[21] X.G. Duan, Z.M. Ao, L. Zhou, H.Q. Sun, G.X. Wang, S.B. Wang, Occurrence of radical and non-radical pathways from carbocatalysts for aqueous and nonaqueous catalytic oxidation, Appl. Catal., B, 188 (2016) 98–105.

[22] M.M. Mian, G.J. Liu, B. Fu, Conversion of sewage sludge into environmental catalyst and microbial fuel cell electrode material: a review, Sci. Total Environ., 666 (2019) 525–539.

[23] W. Oh, T. Lim, Design and application of heterogeneous catalysts as peroxydisulfate activator for organics removal: an overview, Chem. Eng. J., 358 (2019) 110–133.

[24] N. Kojima, A. Mitomo, Y. Itaya, S. Mori, S. Yoshida, Adsorption removal of pollutants by active cokes produced from sludge in the energy recycle process of wastes, Waste Manage., 22 (2002) 399–404.

[25] A. Wießner, M. Remmler, P. Kuschk, U. Stottmeister, The treatment of a deposited lignite pyrolysis wastewater by adsorption using activated carbon and activated coke, Colloids Surf., A, 139 (1998) 91–97.

[26] M. Ahmad, A.U. Rajapaksha, J.E. Lim, M. Zhang, N. Bolan, D. Mohan, M. Vithanage, S.S. Lee, Y.S. Ok, Biochar as a sorbent for contaminant management in soil and water, a review, Chemosphere, 99 (2014) 19–33.

[27] F.Y. Li, F.L. Duan, W.C. Ji, X.Y. Gui, Biochar-activated persulfate for organic contaminants removal: efficiency, mechanisms and

influencing factors, Ecotoxicol. Environ. Saf., 198 (2020) 110653, doi: 10.1016/j.ecoenv.2020.110653.

[28] P.P. Zhang, Y.Y. Yang, X.G. Duan, Y.J. Liu, S.B. Wang, Density functional theory calculations for insight into the heterocatalyst reactivity and mechanism in persulfate-based advanced oxidation reactions, ACS Catal., 11 (2021) 11129–11159.

[29] W.S. Chen, Y.P. Guo, X. Mi, Y. Yu, G.T. Li, Enhanced adsorptive removal of methylene blue by low-temperature biochar derived from municipal activated sludge, Desal. Water Treat., 188 (2020) 257–265.

[30] M. Abdulkarim, F.A. Al-Rub, Adsorption of lead ions from aqueous solution onto activated carbon and chemically-modified activated carbon prepared from date pits, Adsorpt. Sci. Technol., 22 (2004) 119–134.

[31] V. Strelko, D.J. Malik, M. Streat, Characterisation of the surface of oxidised carbon adsorbents, Carbon, 40 (2002) 95–104.

[32] G.T. Li, K.H. Wong, X.W. Zhang, C. Hu, J.C. Yu, R.C.Y. Chan, P.K. Wong, Degradation of Acid Orange 7 using magnetic AgBr under visible light: the roles of oxidizing species, Chemosphere, 76 (2009) 1185–1191.

[33] X. Cheng, H.G. Guo, Y.L. Zhang, X. Wu, Y. Liu, Non-photochemical production of singlet oxygen via activation of persulfate by carbon nanotubes, Water Res., 113 (2017) 80–88.

[34] B.C. Huang, J. Jiang, G.X. Huang, H.Q. Yu, Sludge biochar-based catalysts for improved pollutant degradation by activating peroxymonosulfate, J. Mater. Chem. A, 6 (2018) 8978–8985.

[35] M. Periasamy, M. Thirumalaikumar, Methods of enhancement of reactivity and selectivity of sodium borohydride for applications in organic synthesis, J. Organomet. Chem., 609 (2000) 137–151.

[36] S.S. Fan, Y. Wang, Z. Wang, J. Tang, J. Tang, X.D. Li, Removal of methylene blue from aqueous solution by sewage sludge-derived biochar: adsorption kinetics, equilibrium, thermodynamics and mechanism, J. Environ. Chem. Eng., 5 (2017) 601–611.

[37] H.R. Yuan, T. Lu, H.Y. Huang, D.D. Zhao, N. Kobayashi, Y. Chen, Influence of pyrolysis temperature on physical and chemical properties of biochar made from sewage sludge, J. Anal. Appl. Pyrolysis, 112 (2015) 284–289.

[38] X.D. Cao, W. Harris, Properties of dairy-manure-derived biochar pertinent to its potential use in remediation, Bioresour. Technol., 101 (2010) 5222–5228.

[39] E.B. Yang, C.L. Yao, Y.H. Liu, C. Zhang, L.T. Jia, D.B. Li, Z.H. Fu, D.K. Sun, S. Robert Kirk, D.L. Yin, Bamboo-derived porous biochar for efficient adsorption removal of dibenzothiophene from model fuel, Fuel, 211 (2018) 121–129.

[40] Z. Li, Y.Q. Sun, Y. Yang, Y.T. Han, T.S. Wang, J.W. Chen, D.C.W. Tsang, Biochar-supported nanoscale zero-valent iron as an efficient catalyst for organic degradation in groundwater, J. Hazard. Mater., 383 (2020) 121240, doi: 10.1016/j.jhazmat.2019.121240.

[41] S. Altenor, B. Carene, E. Emmanuel, J. Lambert, J. Ehrhardt, S. Gaspard, Adsorption studies of methylene blue and phenol onto vetiver roots activated carbon prepared by chemical activation, J. Hazard. Mater., 165 (2009) 1029–1039.

[42] M. Pumera, B. Šmíd, K. Veltruská, Influence of nitric acid treatment of carbon nanotubes on their physico-chemical properties, J. Nanosci. Nanotechnol., 9 (2009) 2671–2676.

[43] H. Ago, T. Kugler, F. Cacialli, W.R. Salaneck, M.S.P. Shaffer, A.H. Windle, R.H. Friend, Work functions and surface functional groups of multiwall carbon nanotubes, J. Phys. Chem. B, 103 (1999) 8116–8121.

[44] Y.L. Zhao, H. Wang, Structure–function correlations of carbonaceous materials for persulfate-based advanced oxidation, Langmuir, 37 (2021) 13969–13975.

[45] X.G. Duan, H.Q. Sun, S.B. Wang, Metal-free carbocatalysis in advanced oxidation reactions, Acc. Chem. Res., 51 (2018) 678–687.

[46] A. Georgi, F. Kopinke, Interaction of adsorption and catalytic reactions in water decontamination processes, Appl. Catal., B, 158 (2005) 9–18.

[47] P. Neta, R.E. Huie, A.B. Ross, Rate constants for reactions of inorganic radicals in aqueous solution, J. Phys. Chem. Ref. Data, 17 (1988) 1027–1284.

[48] I. Velo-Gala, J.J. López-Peñalver, M. Sánchez-Polo, J. Rivera-Utrilla, Role of activated carbon surface chemistry in its photocatalytic activity and the generation of oxidant radicals under UV or solar radiation, Appl. Catal., B, 207 (2017) 412–423.

[49] S.Y. Yang, X. Yang, X.T. Shao, R. Niu, L.L. Wang, Activated carbon catalyzed persulfate oxidation of Azo dye acid orange 7 at ambient temperature, J. Hazard. Mater., 186 (2011) 659–666.

[50] R.L. Yin, W.Q. Guo, H.Z. Wang, J.S. Du, X.J. Zhou, Q.L. Wu, H.S. Zheng, J.S. Chang, N.Q. Ren, Selective degradation of sulfonamide antibiotics by peroxymonosulfate alone: direct oxidation and non-radical mechanisms, Chem. Eng. J., 334 (2018) 2539–2546.

[51] L.R. Radovic, C. Moreno-Castilla, J. Rivera-Utrilla, Carbon materials as adsorbents in aqueous solutions, Chem. Phys. Carbon, 27 (2001) 227–405.

[52] X. Cheng, H.G. Guo, Y.L. Zhang, X. Wu, Y. Liu, Non-photochemical production of singlet oxygen via activation of persulfate by carbon nanotubes, Water Res., 11 (2017) 80–88.

[53] Y. Zhou, J. Jiang, Y. Gao, J. Ma, S.Y. Pang, J. Li, X.T. Lu, L.P. Yuan, Activation of peroxymonosulfate by benzoquinone: a novel non-radical oxidation process, Environ. Sci. Technol., 49 (2015) 12941–12950.

[54] X.R. Zhou, Z.T. Zeng, G.M. Zeng, C. Lai, R. Xiao, S.Y. Liu, D.L. Huang, L. Qin, X.G. Liu, B.S. Li, H. Yi, Y.K. Fu, L. Li, M.M. Zhang, Z.H. Wang, Insight into the mechanism of persulfate activated by bone char: unraveling the role of functional structure of biochar, Chem. Eng. J., 401 (2020) 126–127.

[55] X. Cheng, H.G. Guo, Y.L. Zhang, G.V. Korshin, B. Yang, Insights into the mechanism of non-radical reactions of persulfate activated by carbon nanotubes: activation performance and structure-function relationship, Water Res., 157 (2019) 406–414.

[56] G. Song, F.Z. Qin, J.F. Yu, L. Tang, Y. Pang, C. Zhang, J.J. Wang, L.F. Deng, Tailoring biochar for persulfate-based environmental catalysis: impact of biomass feedstocks, J. Hazard. Mater., 424 (2022) 127663, doi: 10.1016/j.jhazmat.2021.127663.

[57] D. Ouyang, Y. Chen, J.C. Yan, L.B. Qian, L. Han, M.F. Chen, Activation mechanism of peroxymonosulfate by biochar for catalytic degradation of 1,4-dioxane: important role of biochar defect structures, Chem. Eng. J., 370 (2019) 614–624.
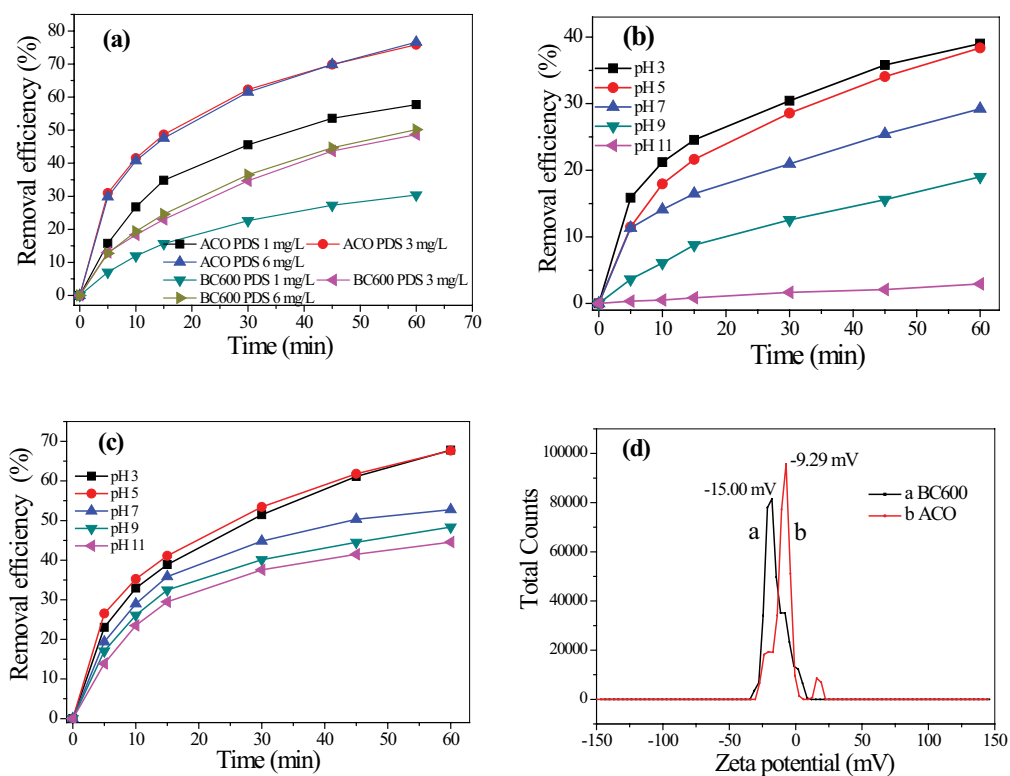
Supporting information

Fig. S1. Effect of PDS dose and solution pH on tetracycline degradation. (a) PDS dose, (b) BC600, (c) ACO and (d) zeta potential of BC600 and ACO.
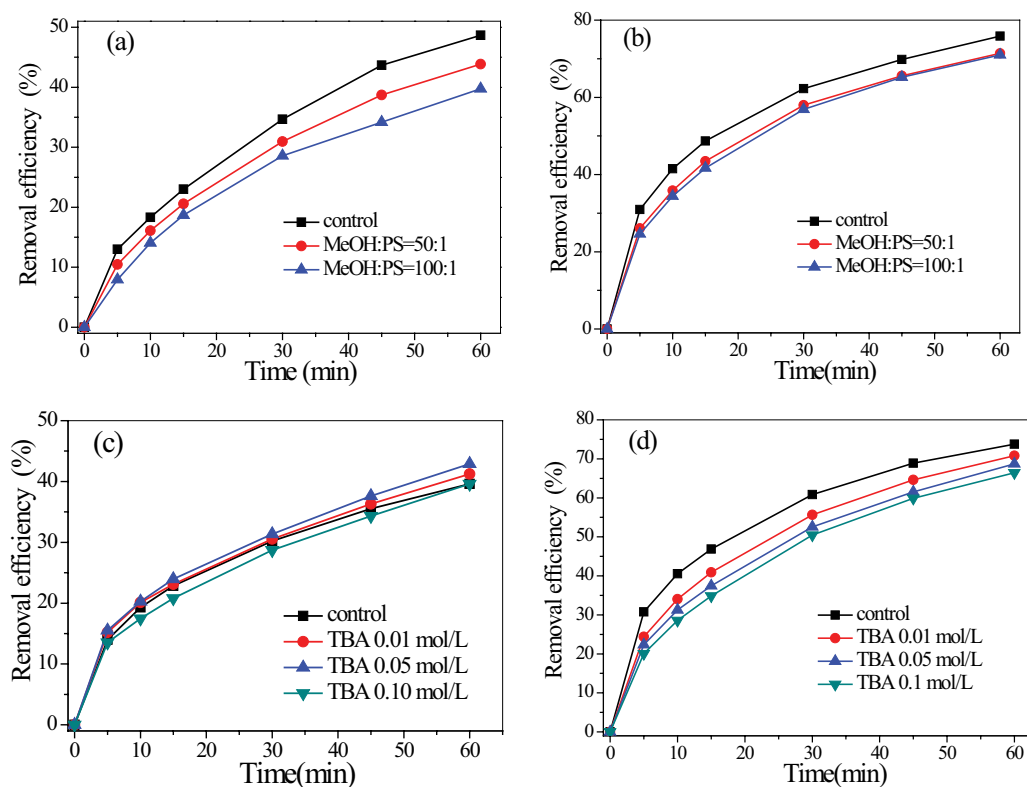

Fig. S2. Effect of MeOH (a,b) and tert-butyl alcohol (c,d) quenching on tetracycline degradation. BC600 (a,c) and ACO (b,d).
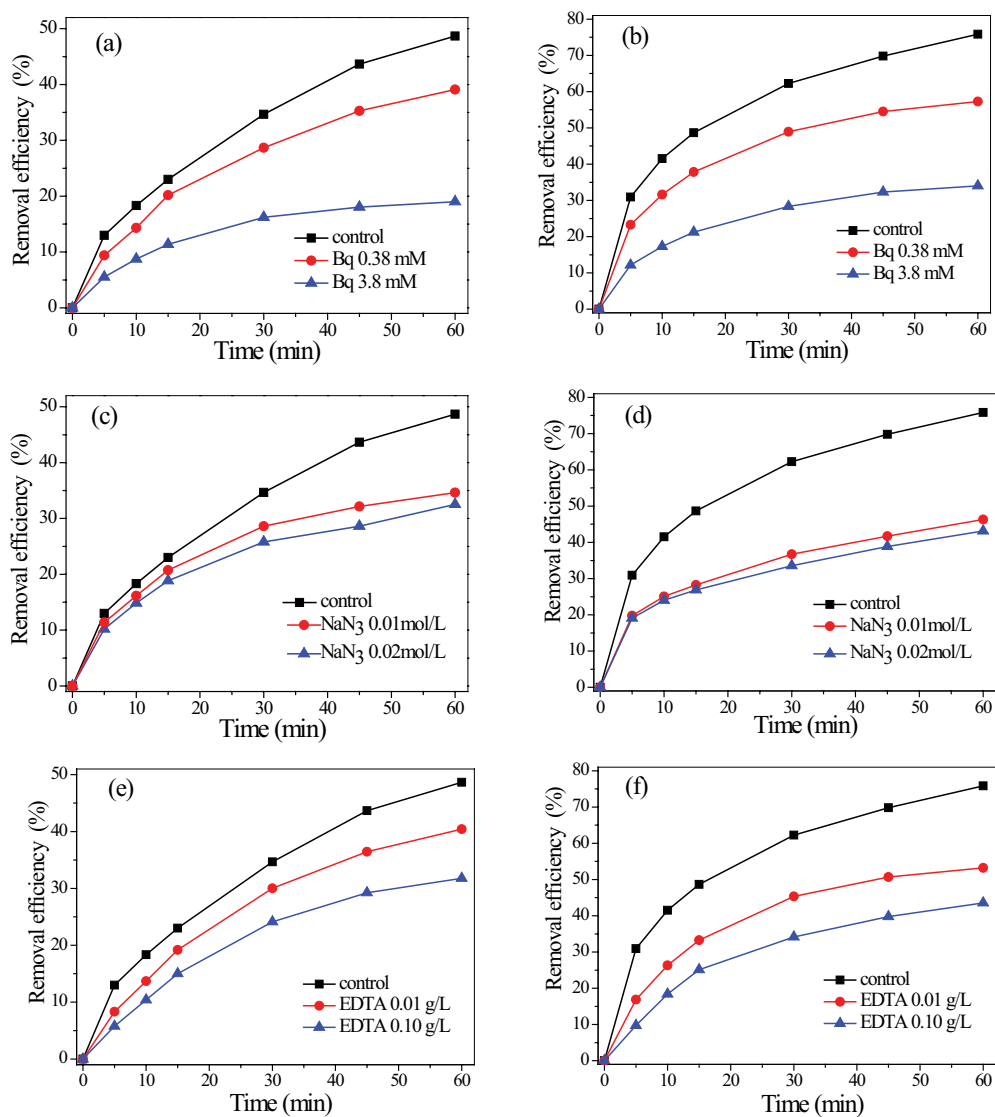
Fig. S3. Effect of Bq (a,b), NaN₃ (c,d), and EDTA (e,f) quenching on tetracycline degradation. BC600 (a,c,e) and ACO (b,d,f).
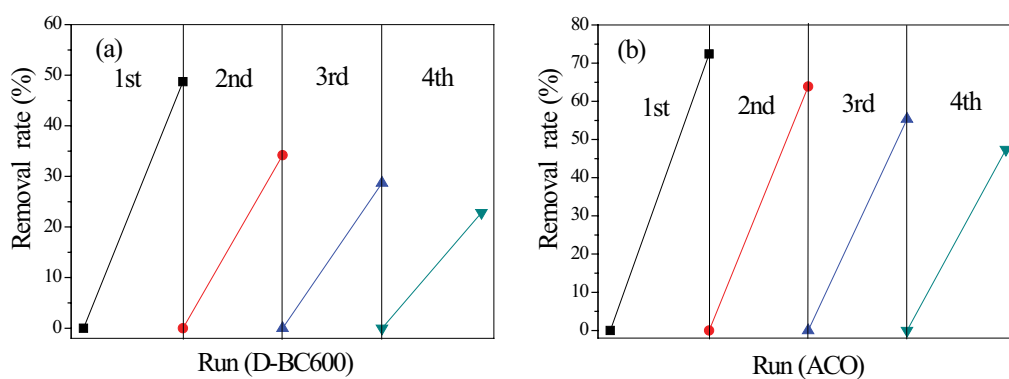

Fig. S4. Reusability of both BC600 and ACO in the PDS catalytic process.